NeuroImage 52 (2010) 985–994

Contents lists available at ScienceDirect

NeuroImage

journal homepage: www.elsevier.com/locate/ynimg

The relationship between structural and functional connectivity: Graph theoretical analysis of an EEG neural mass model

S.C. Ponten [a,b,*], A. Daffertshofer [c], A. Hillebrand [a], C.J. Stam [a]

[a] Department of Clinical Neurophysiology, VU University Medical Center, de Boelelaan 1117, 1081 HV, Amsterdam, The Netherlands
[b] Department of Neurology, VU University Medical Center, de Boelelaan 1117, 1081 HV, Amsterdam, The Netherlands
[c] Research Institute MOVE, VU University, van der Boechorstraat 9, 1081 BT, Amsterdam, The Netherlands

ARTICLE INFO

Article history:
Received 2 December 2008
Revised 14 October 2009
Accepted 15 October 2009
Available online 22 October 2009

Key words:
EEG
Modeling
Synchronization
Graph theory
Small-world networks
Complexity
Functional connectivity

ABSTRACT

We investigated the relationship between structural network properties and both synchronization strength and functional characteristics in a combined neural mass and graph theoretical model of the electroencephalogram (EEG). Thirty-two neural mass models (NMMs), each representing the lump activity of reasonably large groups of interacting excitatory and inhibitory neurons, were reciprocally and excitatory coupled using random rewiring as described by Watts and Strogatz. Numerical analysis of the network revealed an abrupt transition towards a synchronized state as a function of increasing coupling strength α. Synchronization increased with increasing degree and decreasing regularity of the network. Parameters of the functional network showed a diverse dependency on structural connectivity: normalized clustering coefficient γ and path length λ increased with increasing α. For sufficiently large α, however, γ decreased with increasing rewiring probability p, while λ increased. Hence, a structured functional network exists despite the randomness of the underlying structural network. That is, patterns of functional connectivity are influenced by patterns of the corresponding structural level but do not necessarily agree with those.

Introduction

A central problem in neuroscience is the question how communication takes place between distributed parts of the brain. This problem is relevant for both microscopic interactions between single neurons and large-scale communication between macroscopic brain areas (Lopes da Silva, 1991; Friston, 2001; Le Van Quyen, 2003; Stephan et al., 2008). There is increasing evidence that (both local and long-range) synchronization of oscillatory neural activity is an important mechanism for interregional exchange of information (Varela et al., 2001; Schnitzler and Gross, 2005). At the macroscopic level synchronization can be studied using functional imaging techniques like electroencephalography (EEG) and magneto-encephalography (MEG) (Sporns et al., 2000; Stam et al., 2003). Statistical interdependencies, e.g., the strength of synchronization between neural activity, can reflect functional interactions or correlations between brain regions, quantified as 'functional connectivity' (Aertsen et al., 1989; Lee et al., 2003). Over the years, many studies have been devoted to characterizing functional connectivity during resting-state as well as during various cognitive tasks (e.g., Varela et al., 2001; Le Van Quyen et al., 2001; David et al., 2003). While spatial patterns of functional connectivity in healthy subjects during resting-state are fairly consistent, several neuropsychiatric disorders may cause severe disturbances of functional connectivity (Babiloni et al., 2004; Stam et al., 2005; Posthuma et al., 2005; Damoiseaux et al., 2006; Uhlhaas and Singer, 2006; Smit et al., 2007). Studies of functional connectivity yield a bewildering amount of descriptive measures for the interactions between large numbers of brain regions. Combining such imaging data with mathematical models of interconnected brain regions helps to select or assort these measures by unraveling causal interactions, often referred as 'effective connectivity' (Friston, 2001; Ursino et al., 2007). The link between data and models, however, is typically restricted to a small number of interacting brain regions, whereas the human brain is known for its large, complex network structure and a high-dimensional, complex dynamics. Here we address this complexity by studying the functional dynamics of the networks. In particular, we investigate the relation between spatial patterns of functional connectivity and the structure or topology of the underlying anatomical network.

The technical advance in computational capacity made simulating large networks of single or multi-compartment neurons possible (Izhikevich and Edelman, 2008). Such simulations suggested a high level of biological realism, but due to their magnitude their explanatory value remains limited (Deco et al., 2008). To understand the qualitative relationship between macroscopically recorded signals and the underlying, structural connectivity, modeling local groups of neurons in terms of average properties like their mean voltage and firing rates appears more efficient. This macroscopic (mean-field-like)

* Corresponding author. VU University Medical Center, P.O. Box 7057, 1007 MB, Amsterdam, The Netherlands. Fax: +31 20 4444816.
E-mail address: sc.ponten@vumc.nl (S.C. Ponten).

1053-8119/$ – see front matter © 2009 Elsevier Inc. All rights reserved.
doi:10.1016/j.neuroimage.2009.10.049

approach has indeed a long tradition and is typically referred to as lumped or neural mass models (NMMs) (Wilson and Cowan, 1972; Lopes da Silva et al., 1974, 1976; Freeman, 1978; Jansen and Rit, 1995; Robinson et al., 2005; Deco et al., 2008). NMMs have been used to study the origin of alpha rhythm, evoked potentials, pathological brain rhythms, and the transition between normal and epileptic activity (Jansen and Rit, 1995; Lopes da Silva et al., 1997; Valdes et al., 1999; Stam et al., 1999a,b; Wendling et al., 2005; David et al., 2005). While a few studies considered small networks of two or three interconnected NMMs (van Rotterdam et al., 1982; Wendling et al., 2001; David and Friston, 2003; Ursino et al., 2007), more recently, a larger model of interconnected NMM has been developed, with interregional connections based on anatomical information of diffusion weighted MRIs (Sotero et al., 2007). This study revealed to what degree NMMs, in combination with realistic connectivity patterns, may reproduce EEG rhythms generated in spatially distributed brain regions. Functional relevance and meaning, however, await to be addressed. Honey and colleagues (2007, 2008, 2009) as well as Zhou and colleagues (2007) investigated the relationship between structural and functional connectivity, suggesting that functional connectivity may indeed resemble aspects of structural connectivity. In both studies, a fixed structural architecture was implemented based on either the cortical structure of the cat (Zhou and others) or the macaque neocortex (Honey and colleagues). Yet it is unclear how variations in the network properties at the structural level may affect the synchronization strength and more global network characteristics at the functional level.

Complex networks can be modeled and analyzed using graph theory. Random (Erdös-Rényi) graphs in combination with a specific structure yield so-called small-world networks (Watts and Strogatz, 1998) or scale-free networks (Barabasi and Albert, 1999). In brief, small-world networks are characterized by strong local connectedness (quantified by a large clustering coefficient C) and by pronounced global integration (quantified by a short path length L). This combination can be found in a wide range of networks in nature (Wang and Chen, 2003). Several studies, varying from *C. elegans* to cat, macaque, and humans, have shown that anatomical networks in the brain are characterized by strong local clustering and short path lengths (Stephan et al., 2000; Hilgetag et al., 2000; Sporns and Zwi, 2004; He et al., 2007). Network analysis applied to patterns of functional connectivity from the microscopic neural to the macroscopic EEG, MEG, and fMRI level (Eguiluz et al., 2005; Reijneveld et al., 2007; Yu et al., 2008) has also shown small-world characteristics. Interestingly, in various neurological disorders these characteristics appear disrupted, mostly in the direction of a more random network organization; see Table 1 for an overview (Micheloyannis et al., 2006; Ponten et al., 2007; Stam et al., 2007a). While studies on pathology do emphasize the relevance of complex networks for normal functioning, one may argue that the reported differences in network parameters between healthy subjects and patients merely reflect changes in the underlying anatomy. However, to date it is an open question how network properties at the structural level affect the dynamics of neural synchronization at the functional level, or the functional network topology.

Table 1
EEG/MEG studies concerning small-world analysis in various diseases.

Study	Disease	γ = C/C-s		λ = L/L-s		K	N
		Control	Disease	Control	Disease		
Micheloyannis et al. (2006)	Schizophrenia[a]	1.9	1.7	1.1	1.2	5	28
Stam et al. (2007a,b)	Dementia[b]	1.9	1.6	1.1	1.1	3	21
Bartolomei et al. (2006)	Brain tumor[c]	5.2	4.2	1.7	1.4	10	149
Ponten et al. (2007)	Absences[d]	1.4	1.7	1.0	1.3	6	21
Smit et al. (2007)	Genetic study	1.5		1.1		5	17

[a] Alpha2 band (10–13 Hz).
[b] Beta band (13–30 Hz).
[c] Theta band (4–8 Hz), diseased were patients with right-sided tumors.
[d] Control is the pre-ictal period; disease is ictal period. Broad filtered signal (1–48 Hz).

To explore the relationship between structural network properties and both synchronization strength and functional network properties, we used common alpha rhythm NMMs (Lopes da Silva et al., 1974) as nodes in the structural network and designed different network architectures via the rewiring algorithm proposed by Watts and Strogatz (1998). Synchronization between multi-channel EEG signals as generated by the model was quantified as phase coherence (Stam et al., 2007b). The resulting spatial phase coherence distributions were subject to network analysis yielding functional connectivity measures that, in turn, were related to underlying structural network properties.

Methods

The neural mass model

We used an NMM originally designed to mimic the alpha rhythm (Lopes da Silva et al., 1974; Zetterberg et al., 1978) as basic unit of our model. This NMM is based on early works of Wilson and Cowan (1972) and considers the average activity in relatively large groups of interacting excitatory and inhibitory neurons.[1] As sketched in Fig. 1a the excitatory and inhibitory neural populations of an NMM can be characterized by their average membrane potentials $V_e(t)$ and $V_i(t)$, and by their pulse densities, i.e., the number of cells firing per unit time $E(t)$ and $I(t)$. A non-linear transfer function $S[V]$ relates the membrane potentials to their corresponding pulse densities. Excitatory neurons are coupled with inhibitory populations with strength G_1 and vice versa with strength G_2. The excitatory postsynaptic potential (EPSP) and inhibitory postsynaptic potential (IPSP) are given by the impulse responses:

$$h(t) = \begin{cases} A\left(e^{-at} - e^{-bt}\right) & \text{for } t \geq 0 \\ 0 & \text{otherwise} \end{cases}; \quad (1)$$

with $A = 1.6$ mV, $a = 55\ s^{-1}$, $b = 605\ s^{-1}$ for $h(t) = h_e(t)$, and $A = 32$ mV, $a = 27.5\ s^{-1}$, $b = 55\ s^{-1}$ for $h(t) = h_i(t)$. Form and parameters were adopted from Zetterberg and others (1978) who suggested the transfer function to be exponential:

$$S[V] = g\begin{cases} e^{q(V-V_0)} & \text{for } V \leq V_0 \\ 2 - e^{-q(V-V_0)} & \text{otherwise} \end{cases}; \quad (2)$$

with $q = 0.34\ (\text{mV})^{-1}$, $V_0 = 7$ mV, $g = 25\ s^{-1}$. The coupling constants were set to $G_1 = 32$ and $G_2 = 3$ (cf. Lopes da Silva et al., 1974). Finally, we added subcortical input pulses $P_{\text{ext}}(t)$ to the excitatory population of an NMM; on average $P_{\text{ext}}(t)$ contained 550 action potentials per second but the rate varies randomly (the pulse rate variation was realized using Gaussian white noise with standard deviation of 0.1 potentials per second).

We combined $N = 32$ NMMs. If present the coupling between two NMMs was always reciprocal and excitatory: $E(t)$ of an NMM was used as input for the impulse response $h_e(t)$ of the excitatory neurons of a coupled NMM, and vice versa (see Fig. 1b for the case of two coupled NMMs). Following Ursino and colleagues (2007), we used a finite transfer time ($\tau = 2$ ms) and a coupling strength α between NMMs and we considered a homogeneous network in

[1] Spatial effects are ignored in the NMM but will be introduced by coupling several NMMs.

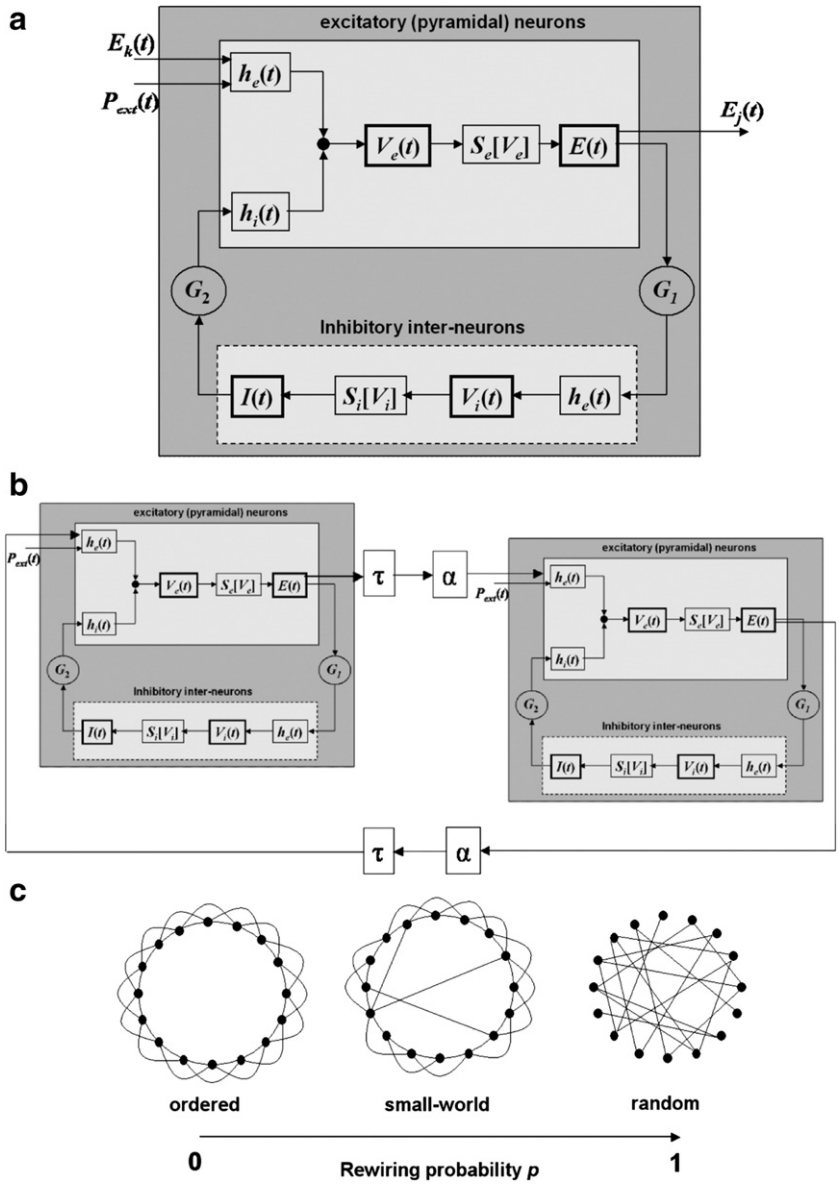

Fig. 1. (a) Basic scheme of neural mass model (NMM) implemented at every node. (b) Coupling scheme between two NMMs. τ = time delay between the nodes, α = the coupling strength between two nodes. (c) Three fundamental network topologies for the model of coupled NMMs; after Watts and Strogatz (1998).

which all NMMs received similar but individual (i.e., pair-wise uncorrelated) inputs $P_{\text{ext},1}(t)$, $P_{\text{ext},2}(t)$, $P_{\text{ext},3}(t)$, and so on.

The algorithm of Watts and Strogatz (1998) was used to design the NMMs network: starting with a network on a ring, in which each network node or NMM was coupled to its k nearest neighbors ($k/2$ on each side), connections (edges) were selected at random with probability p and attached to randomly chosen other NMMs. We note that by varying the rewiring probability p from 0 to 1 one can recover the 'full' range of network types from regular via small-world to purely random (see Fig. 1c). The NMM model was adopted from Schuuring (1988) and Stam (1999a), extended to multiple NMMs and integrated in the DIGEEGXP software package (version 2.0; written by one of the authors, C.J.S.). This software is also used for EEG/MEG analysis (see below). The average membrane potential $V_e(t)$ of the excitatory neurons served as signal per node. The sample frequency was set to 500 Hz, the initial 5000 samples of each simulation were discarded to avoid transients, and the consecutive 4096 samples (8.19 s) were used for further analysis. We chose these parameters in order to mimic characteristics of clinical EEG and MEG studies (e.g., Stam et al., 2007a, 2008).

Phase coherence

We quantified synchronization between NMMs at different nodes via their relative phase. Phase entrainment between two units requires their phase difference to be bounded. That is, if ϕ_n and ϕ_m denote the phases of two signals, and ϕ_{nm} the corresponding generalized phase difference or relative phase, the P:Q phase synchronization can be found as

$$|\phi_{nm}^{PQ}| = |P\phi_n - Q\phi_m| < \text{const}, \tag{3}$$

with P and Q integers. Using this general definition, phase coherence can be determined for oscillatory but also for noisy and chaotic signals; see Rosenblum and colleagues (1996) for an in-depth discussion. Here, we confined ourselves to the iso-frequency case by considering only $P=Q=1$, that is, $\phi_{nm}=\phi_n - \phi_m$. We computed the instantaneous phase of the signal under study $x(t)$ via its analytical signal $z(t)=x(t)+ix_H(t)$, where $x_H(t) = \frac{1}{\pi}\left[x(t)*t^{-1}\right]$ denotes the Hilbert transform of $x(t)$, i.e., the convolution of $x(t)$ with the hyperbolic function. The average membrane potential $V_e(t)$

of the excitatory neurons was used here as signal $x(t)$. By construction the analytical signal $z(t)$ is complex-valued and one can translate it to its corresponding instantaneous amplitude $A(t)$ and instantaneous phase $\phi(t)$ in terms of $z(t)=A(t)e^{i\phi(t)}$. In turn, the phase reads $\phi(t)=\arctan'(x_H(t)/x(t))$, where arctan′ denotes the quadrant corrected inverse tangent. As said, from the phases of two signals, i.e., $x_n(t)$ and $x_m(t)$, we computed the instantaneous relative phase $\phi_{nm}(t)$ and tested its boundedness. We adopted the notion of phase coherence described by Mormann and colleagues (2000); see also Mardia (1972). That is, in view of its 2π-periodicity, phase differences were computed on the circle and averaged over time so that the mean resultant length R_{nm} served to quantify synchrony

$$R_{nm}=\left|\frac{1}{T}\right|\int_0^T e^{i\phi_{nm}(t)}dt\Bigg|; \tag{4}$$

T denotes the time interval during which the signals are recorded. The case of perfect phase locking yields $R_{nm}=1$, whereas in the case of a uniform distribution of phases on the unit circle R_{nm} will vanish.[2] To calculate the mean phase coherence of the entire network with N nodes, we computed the pair-wise phase coherence via Eq. (4) and averaged over pairs by means of

$$\overline{R}=\frac{1}{N-1}\sum_{n=1}^{N-1}\left(\frac{1}{N-n}\sum_{m=n+1}^{N}R_{nm}\right) \tag{5}$$

Network analysis

Graphs generally serve as abstract representation of a network. A graph consists of a set of vertices (or nodes) and a set of edges or links, defined via the connectivities between vertices. Given N vertices the latter is typically summarized as an $N\times N$ connectivity matrix (i.e., matrix elements are defined by the connectivity between vertices n and m). The corresponding adjacency matrix A summarizes the discrete structure of the graph (Boccaletti et al., 2006): when an edge exists between two vertices n and m, then the corresponding coefficient of the adjacency matrix, A_{nm}, is equal to 1, otherwise it vanishes. Furthermore, the number of edges connecting to ('incident on') a vertex n is called the degree k_n of this vertex. The average degree of the entire graph is denoted by K (here K_s was used for the structural network and K_f for the functional network).

We applied network analysis to the level of structural connectivity, i.e., the links between the 32 NMMs as described in the subsection neural mass model, as well as to the functional connectivity consisting of statistical interdependencies between output signals of the NMMs, quantified via the just explained phase coherence, here also referred to as synchronization. That is, each NMM formed a vertex in the graph. For the structural network the adjacency matrix was subsequently generated by wiring in the Strogatz and Watts model (see above; we note that the rewiring preserves the average degree K_s) and for the functional network the connectivity matrix was generated from the connections as computed via the phase coherence between NMMs at vertices n and m. With the resulting $N\times N$ connectivity matrix of phase coherence values R_{nm}, with $0\leq R_{nm}\leq 1$, we defined the adjacency matrix A using a threshold[3] so that $R_{nm}>$threshold yielded an edge i.e., $A_{nm}=1$, whereas $R_{nm}\leq$threshold implied that the vertices n and m were not connected, i.e., $A_{nm}=0$. The threshold was either chosen such that the resulting graph had a fixed average degree K_f (starting at zero the threshold was increased in small steps until the resulting graph had the desired average degree K_f) or so as to include only significant connections (i.e., only large phase coherence values were set to 1, others to 0); see the end of this subsection for more details.

As indicated in the Introduction, we quantified the local and global structure of graphs via their mean clustering coefficient C and the characteristic path length L. In general, the clustering coefficient C_n of a vertex n with degree k_n is defined as the ratio of the number of existing edges ($\#_n$) between neighbors of n (a vertex m is called a neighbor if $A_{nm}=1$) and the maximum possible number of edges. This can be formalized as

$$C_n=\frac{2\#_n}{k_n(k_n-1)}=\frac{1}{k_n(k_n-1)}\sum_{m=1}^{N}\sum_{o=1}^{N}A_{mn}A_{no}A_{om}. \tag{6}$$

That is, C_n is an index of local structure, which has been interpreted as a measure of resilience to random error (in case vertex n is lost its neighbors remain connected if C_n is large). C is the mean clustering coefficient of the graph, that is,

$$C=\frac{1}{N}\sum_{n=1}^{N}C_n \tag{7}$$

The path length L_{nm} between two vertices n and m is the minimal number of edges that have to be passed to connect n and m. The mean shortest path length L of a graph (or just its path length) is the mean L_{nm} between all possible pairs of vertices. We note that using the harmonic mean allows for inclusion of isolated vertices (for which $L_{nm}\to\infty$, see Newman, 2003). That is, we used

$$L^{-1}=\frac{1}{N(N-1)}\sum_{n=1}^{N}\sum_{\substack{m=1\\ n\neq m}}^{N}\frac{1}{L_{nm}}. \tag{8}$$

C and L were compared to the average values obtained for ensembles of surrogate networks. These surrogate networks were constructed for each graph by randomly shuffling edges, preserving the degree, the degree distribution, and the symmetry of the graph ($A_{nm}=A_{mn}$). For all simulations we used ensembles of 50 surrogate networks per graph, generated using the method first described by Maslov and Sneppen (2002). Finally, we computed 'normalized' parameters γ and λ as

$$\gamma=C/\langle C_{\text{surrogate}}\rangle \text{ and } \lambda=L/\langle L_{\text{surrogate}}\rangle, \tag{9}$$

which served to assess network topologies.

We briefly return to the issue of converting the connectivity matrix to binary adjacencies. The use of a fixed average degree in the reconstruction of the network topology from the connectivity matrices may present problems when all, or a considerable number of, the pair-wise phase coherence values are not significant. This is likely to occur for low values of the coupling strength (see below). In this case the resulting edges may just connect random vertices, biasing estimates of topology towards that of a random graph. That is, the normalized values defined in Eq. (9) will generally tend towards one. We therefore supplemented the analysis by assigning edges only to those nodes whose phase coherence exceed the following criterion: we computed the pair-wise phase coherences in a network of uncoupled NMMs (i.e., coupling strength equal to 0), estimated its mean, $\overline{R}_{\text{uncoupled}}$, and standard deviation, $\sigma_{R,\text{uncoupled}}$, and considered only those values that exceeded $\overline{R}_{\text{uncoupled}}+3\sigma_{R,\text{uncoupled}}$ to be significant. We note that both threshold definitions have their caveats. While the fixed-degree approach may yield a bias by misinterpreting non-significant connectivities as random edges, the threshold via significance approach requires the comparison of networks of

[2] R_{nm} is insensitive to changes in amplitudes and only depends on the phase relations between the two signals. Notice that R_{nm} as defined in Eq. (4) reflects both zero phase lag as well as non-zero phase lag coupling of the phases between two signals.

[3] Using adjacency instead of connectivity yields so-called unweighted graphs, i.e., binary connections. We note that our analysis can also be applied for weighted graphs but results are not expected to differ qualitatively.

different size (here number of edges). An in-depth discussion of this important issue, however, is beyond the scope of the current study but will be discussed elsewhere (van Wijk et al., in preparation). Here, we used both approaches and discuss the results in parallel.

Results

Fully connected network

To get a feel for the synchronization characteristics of the NMMs we first investigated the fully connected network, i.e., the degree of every vertex equals the average degree of the structural network, $K_s = N - 1$. We expected to find coherent states beyond a critical coupling strength indicating the presence of a spontaneous switch in synchrony similar to the phase transition in the well-known Kuramoto model of weakly coupled phase oscillators (Kuramoto, 1975). To allow for a proper comparison with this seminal model, we incorporated an additional random factor, namely, a small but fixed variation in the natural frequency of the participating oscillators. Here, we only modified the coupling constant G_2, which links inhibitory neurons with excitatory ones, while all other parameters remained identical for all NMMs (for the explicit values see Methods section). That is, we defined for every vertex n the coupling $G_{2,n} = \left(1 + \sigma^2_{G_2} \cdot \Gamma_n\right) G_2^{(0)}$ with $0 \leq \sigma^2_{G_2} \leq 1$ and Γ_n as a randomly picked number from the interval $[-1, 1]$. We varied the coupling strength between the 32 NMMs. For each value of $\sigma_{G_2}{}^2$, the model was simulated 10 times and the mean phase coherence $\overline{R}$ was computed (see Fig. 2). We found a transition to a partially synchronized state (with episodes of coherence between subsets of NMMs) at about $\alpha = 0.12$ and a second switch at about $\alpha = 0.6$ to a fully synchronized state in the case of identical NMMs (see also Supplementary Fig. 1). Recall that although the NMMs were identical they still receive different random inputs $P_{\text{ext},i}(t)$. For $\sigma^2_{G_2} = 0.5$ and $\sigma^2_{G_2} = 1$, the transitions to (incomplete or full) phase synchronization appeared less abrupt and phase synchronization did not reach the same level as for $\sigma^2_{G_2} = 0$. We note that the drop in phase synchronization at intermediate values of α confirms earlier suggestions that increasing coupling may serve to increase asynchrony between the oscillators (Golomb and Hansel, 2000; van Vreeswijk, 2000). Generally though, the fully coupled NMM model did show transitions towards first incompletely then fully synchronized states, which are weakly affected by the variability between individual NMMs.

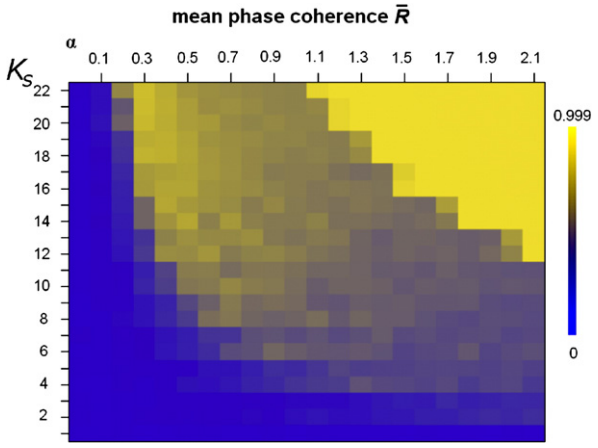

Fig. 3. Mean phase coherence $\overline{R}$ as a function of coupling strength α and degree K_s. K_s varied between 0 and 22, with increments of 1 and the coupling strength α ranged from 0 to 2.1 with increments of 0.1 ($\sigma_{G_2}{}^2 = 0.2$).The figure depicts averages over 10 model simulations.

Not fully connected network

Next we investigated whether the NMMs still synchronize in the not fully connected network. We varied the average degree K_s and in parallel the coupling strength α (see Fig. 3). We expected that in order to realize synchronization the coupling α had to be larger than for the fully connected structural network. For the sake of legibility we fixed the afore-discussed variation of natural frequencies using $\sigma^2_{G_2} = 0.2$; note that the structural network configuration was ordered ($p = 0$). As depicted in Fig. 3, for $K_s \leq 2$ a transition to a synchronized state was entirely absent. For increasing average degrees of the structural network, however, abrupt transitions to higher values of the mean phase coherence $\overline{R}$ occurred for coupling strengths beyond a critical value. This critical value decreased with increasing K_s. For large values of K_s the network showed again the interesting synchronization behavior, in which a rapid transition

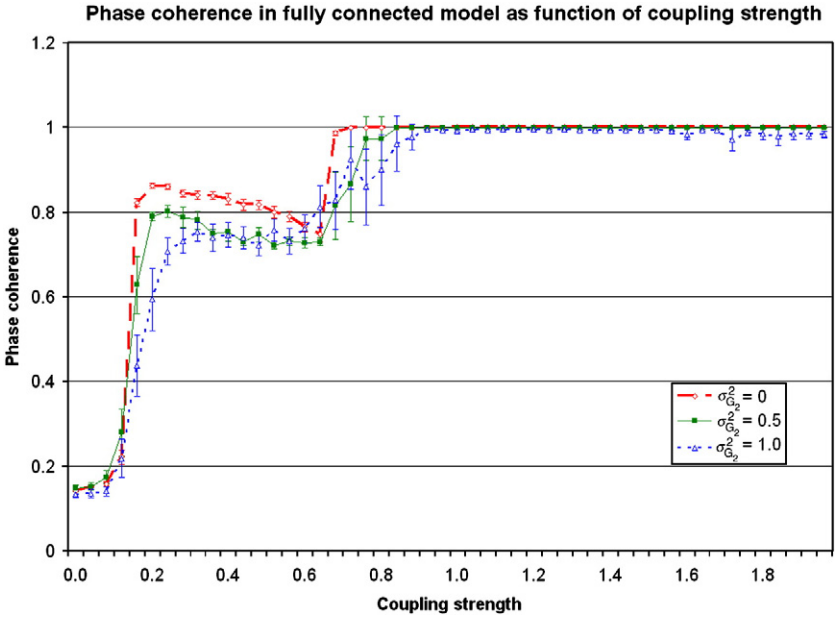

Fig. 2. Mean phase coherence $\overline{R}$ as a function of coupling strength α and $\sigma^2_{G_2}$. α is increased from 0 to 2.0 in steps of 0.04. We used $G_2^{(0)} = 3.0$ and $\sigma^2_{G_2}$ was varied from 0 to 0.5 to 1. We show average values over 10 model simulations (32 NMMs, fully coupled). Error bars show 2× standard error; note that some error bars are too small to visualize.

towards synchronization for increasing α was followed by an intermediate range where synchronization decreased, then pursued by (almost) full synchronization for large α. This non-monotonic change can again be explained by clusters of NMMs with intermediate mean phase coherence $\overline{R}$ that resist full synchronization despite the relatively strong coupling.

Influence of structural network topology on synchronization

Effects of the structural network's topology on the synchronization dynamics was further assessed by modifying the rewiring probability p and the coupling strength α for structural networks with intermediate average degree, and including a small variation of the natural frequency of NMMs ($K_s=6$ and $\sigma_{G_2}{}^2=0.2$, respectively). We found the expected transition towards the synchronized state (Fig. 4), now at a critical coupling strength ($\alpha=0.6$). The highest level of synchronization ($\overline{R}\approx 0.6$ for $\alpha=0.9$ and $p=1.0$) was clearly lower than for the previously discussed, fully connected case (there we had $\overline{R}>0.9$). Interestingly, the rewiring probability p had a fairly weak effect on synchronization, and that only for small probabilities ($0<p<0.1$). The minor impact of rewiring had not been caused by the small number of vertices, because a repetition of the simulations for Fig. 4 with a larger network yielded very similar results ($N=128$, with all other parameters kept constant, see Supplementary Fig. 2). We also repeated this simulation using a different delay (10 ms) and found (results not shown) that the here-discussed transition to synchronized states was rather robust although synchrony required a stronger coupling ($\alpha=0.8$).

Functional versus structural connectivity

Finally we investigated how network analysis applied to the output signals of the model (i.e., functional connectivity) may relate to the structural network parameters α and p. We repeated the simulation described above, and computed the normalized clustering coefficient γ and the normalized path length λ from the functional model output. In Fig. 5a and b, we summarize how spatial patterns of structural connectivity are related to spatial patterns of functional connectivity, for different rewiring probabilities. For $p=0$, i.e., for a regular lattice structure with each NMM connecting to its $K_s=6$ nearest neighboring NMMs on the ring, the mean phase coherence $\overline{R}$ displayed a similar pattern as the structural network with the highest values between nearest neighbors. Given the aforementioned weak impact of the rewiring on the mean phase coherence, which was only visible for small probabilities, we further investigated the case of $p=0.1$. This yielded a few scattered long-distance anatomical connections that were less pronounced in the functional connectivity matrix, when averaged over 10 repeated simulations (note that the structural network was generated once and kept constant afterwards). By contrast, for $p=1.0$, i.e., for a completely random structural connectivity matrix, the functional connectivity matrix also became diffuse, as strong coupling was no longer restricted to nearest neighbors. However, the functional connectivity matrix was still not random, and showed patches (or clusters) of strong phase synchronization (Fig. 5, lower, right panel).

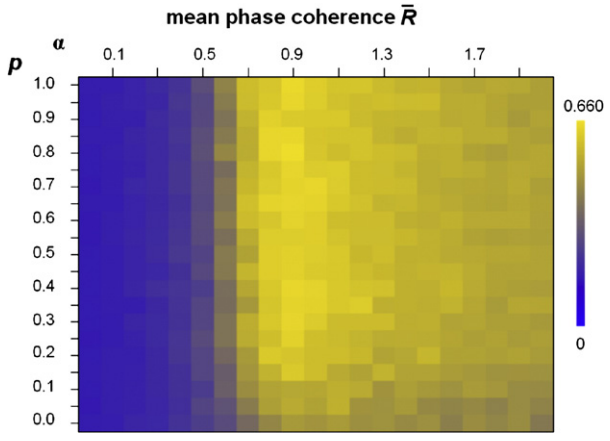

Fig. 4. Mean phase coherence $\overline{R}$ as a function of coupling strength α and rewiring probability p in networks of 32 NMMs with $K_s=6$ and $\sigma_{G_2}{}^2=0.2$. The rewiring probability p was varied from 0 to 1.0 in steps of 0.05 and the coupling strength α is increased from 0.0 to 2.0 in steps of 0.1. Results are average values over 20 repeated simulations.

Results for the functional network parameters γ and λ are shown in Fig. 6a–c. As said we generated the functional adjacency matrix by two different means, using either fixed-degree or significant-connectivity. Starting with the first, Fig. 6a shows the normalized clustering coefficient as a function of coupling strength and rewiring probability. Here the threshold-defining average degree of the functional network was set to be the same as that of the structural network, i.e., $K_f=K_s=6$. To provide a more detailed view of the dynamical characteristics we added three time series representing the time evolution of the membrane potential at single, randomly picked NMMs. For small values of α, the normalized clustering coefficient γ in the functional network remained relatively small ($\gamma\approx 1.5$) prior to phase synchronization onset,[4] and around the onset of synchronization it increased drastically to $\gamma\approx 2.4$. Interestingly, γ reached its largest value for vanishing p and decreased with increasing p. The behavior of λ turned out quite different (Fig 6b): for coupling values below the onset of synchronization, λ was already close to 1 (corresponding to a random network) and increased with increasing α up to $\alpha=1$, after which λ showed an unexpected decrease. Likewise unexpected was a clear increase of λ with increasing rewiring probability p in the vicinity of $\alpha=1$. That is, the average path length of the functional network was much longer than for the surrogate controls, which was most outspoken when the underlying structural network was random.

Defining the threshold via the significance of coherence led to slightly different results. We note that when repeating simulations with the aforementioned criterion ($R_{nm} > \overline{R}_{\text{uncoupled}} + 3\sigma_{R,\text{uncoupled}}$) we had to avoid isolated vertices to guarantee meaningful results. For this sake we tested whether the resulting adjacency matrix contained a connected cluster consisting of at least 90% of all vertices in the network; only then further estimates were included. Equivalent to Eq. (9), the normalized clustering coefficient and path lengths were determined using random control networks. Again, γ and λ were averaged over 10 simulations and depicted as functions of p and α (Fig. 6c, left and right panel, respectively). For small values of α, synchronization was either absent (or not sufficiently strong to form a connected cluster comprising at least 90% of all NMMs). Above $\alpha\approx 0.7$, synchronization was sufficiently strong and widespread to allow for proper reconstructions of functional networks.

The normalized clustering coefficient γ increased with increasing coupling α and decreased for increasing probability p. The normalized path length λ showed a similar dependency on α, but the effect of a change in rewiring probability p was weaker than for the normalized clustering coefficient. Only around $0.8<\alpha<1.1$, the normalized path length λ decreased slightly with increasing p, which was very different to the afore-discussed case of thresholding to the fixed-degree $K_s=6$ (Fig. 6b). Whether this implies that we over- or even misinterpreted the connections when assigning the networks a fixed average degree requires future work. In any case, we can conclude that network properties at the functional level are not necessarily

[4] Onset of synchronization is here defined on the basis of our findings in Fig. 4, where it was shown that with a coupling strength of ≈ 0.6 there is a sudden increase in phase synchronization. It can be seen in Fig. 6a and b that for this value of the coupling strength γ and λ also begin to increase.

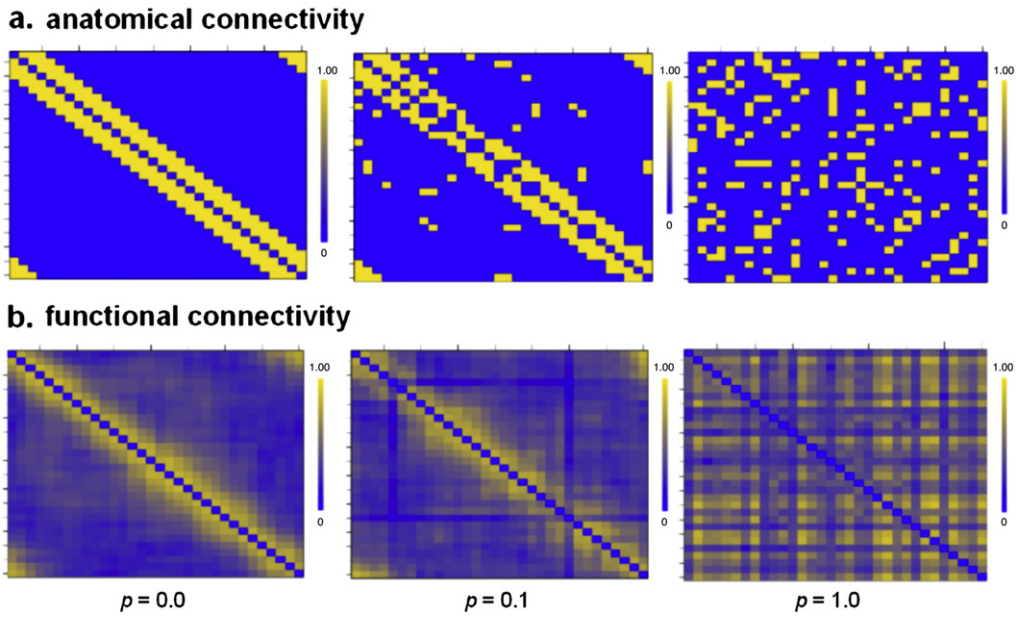

Fig. 5. The relationship between structural and functional connectivity for networks of 32 NMMs, $K_s = 6$, $\sigma_{G_2}{}^2 = 0.2$ and coupling strength $\alpha = 1.2$. The upper row shows the adjacency matrix of the structural network (yellow = 1, blue = 0), the left panel represents a regular network ($p = 0.0$), the middle panel depicts a small-world network ($p = 0.1$) and the right panel shows a random network ($p = 1.0$). The lower row displays the mean phase coherence values between the NMMs, obtained over 10 simulations using the structural networks displayed in the upper row.

identical to network properties of the 'underlying' structural level. The relationship between the two levels is, in general, non-trivial (~not monotonic) and may depend on other parameters like the overall coupling strength.

Discussion

Studying functional connectivity has become a fundamental facet of neurophysiology. To comprehend human brain function, understanding the structural anatomy, the functional connectivity, and their mutual relationship is crucial (Zhou et al., 2007). Neural mass models combined with functional techniques like fMRI, EEG, or MEG appear to be a very promising approach for extending our knowledge of the relationship between structure and function (David and Friston, 2003; Ursino et al., 2007). In a very recent study combining functional MRI and diffusion spectrum imaging tractography and a modeling study Honey and others (2009) demonstrated that although the functional connectivity is variable and is frequently present between regions without direct structural linkage, its strength, persistence and spatial statistics are nevertheless constrained by the large-scale anatomical structure of the human cerebral cortex. We explored the intriguing link between the structural network topology and the network's capacity to synchronize and the resulting functional connectivity. We used a structural network model consisting of 32 NMMs, forming a noise-driven non-linear oscillator each (Lopes da Silva et al., 1974; Zetterberg et al., 1978). The NMMs were coupled in networks with varying topologies (Watts and Strogatz, 1998). The output signals of this model can be considered a first approximation of EEG (using the quasi-static approximation and neglecting some integration effects in the sensors); of course, the issue of how to reconstruct the neuronal signals from externally measured EEG is entirely ignored, that is, only the temporal characteristic of the simulated signals is similar to that in EEG. The resulting functional connectivity between the output signals was quantified using the mean phase coherence.[5]

In agreement with previous studies with weakly coupled phase oscillators (Kuramoto, 1975; Chen et al., 2008), a sudden transition to synchronization was found when the coupling strength α between the NMMs increased. In not fully coupled networks, small-world and random topologies facilitated synchronization. Network parameters of the functional connectivity level depended in a complex way on both the topology and connection strength of the underlying structural network. Importantly, these results show that complex emergent patterns at the functional connectivity level are influenced by, but not necessarily identical to, those of the underlying structural level.

Increasing α in the completely connected structural network led to transition from a desynchronized to a synchronized state for a critical coupling strength. This transition could be modified by randomizing the NMM-internal coupling constant G_2: increasing variability of G_2 caused a less steep increase of synchronization and full synchrony could not be reached any longer. Put differently, the variability of the neural communication can influence the macroscopic functional activity, which we register with EEG or MEG. In support, Zhou and coworkers (2006) showed a steep increase of synchronization by enhancing the coupling strength, and, using the Kuramoto model, similar influences of the variability of the oscillators on synchronization level were also found (Kuramoto, 1975; Chen et al., 2008).

When increasing the number K_s of connections in the NMM network, we found that the transition to the synchronized state occurred with a lower coupling strength α. Hence, a more connected network (a network with a larger average degree) appeared to synchronize earlier. For larger values of K_s, however, we found an interesting sequence of spontaneous transitions, first towards incomplete synchronization, and after a substantial increase of the coupling strength full synchronization emerged. This result disagrees with more recent findings of Zhou and colleagues (2007), who studied synchronization strength using a realistic network model of cat cortical anatomical connectivity, where each cortical area was represented as a NMM. To model the cat cortical network, they used the anatomical connectivity as coupling matrix, which showed small-world characteristics. For both randomized and small-world structured models, they found that the network achieved a high level of synchronization with a strong enough coupling, but without the bimodal pattern we found. Therefore they concluded that the

[5] Other methods (e.g. Ansari-Asl et al., 2006) might give slightly different results, but we do not expect qualitative changes.

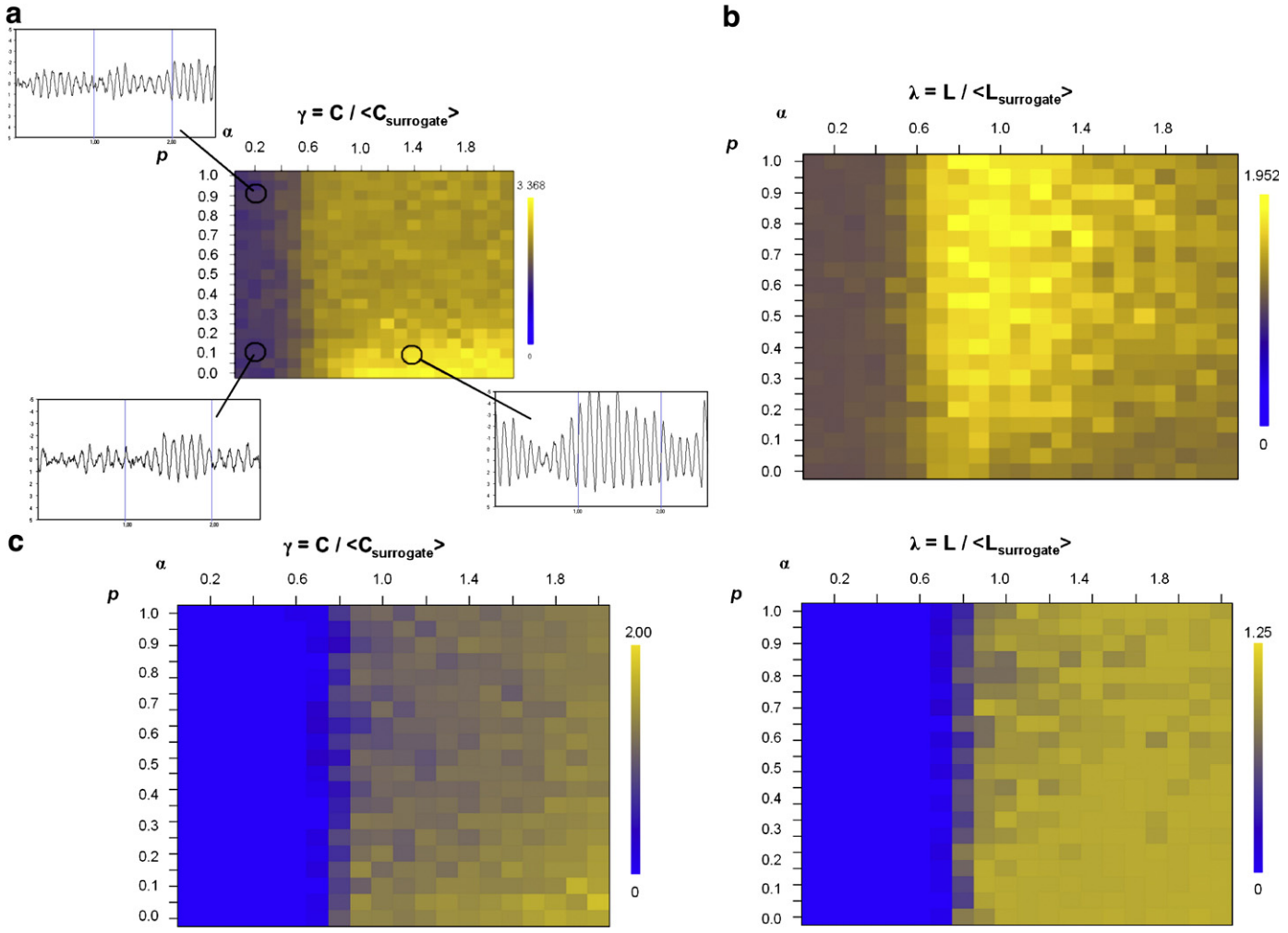

Fig. 6. (a) All parameters match that of the simulations shown in Fig. 4, but now the normalized clustering coefficient γ is plotted instead of the mean phase coherence. Fifty surrogate networks per graph were used. The time series depict the dynamics of randomly selected NMMs with the indicated parameter values. Amplitude was clearly amplified in the synchronized state (lower right panel). Thresholding was realized using a fixed-degree $K_f = 6$. (b) See Figs. 4 and 6a for parameter values; here the normalized path length λ is displayed. (c) Identical parameter settings as in (a) and (b) but thresholding was realized by discarding all non-significant connections. While the dependency on coupling strength of the of clustering coefficient (left panel) and the path length (right panel) largely agree with (a) and (b), respectively, here the dependency on the rewiring probability p is less pronounced.

synchronization patterns or functional dynamics were mainly controlled by the global structural statistics of the nodes.

Very recently Brede (2008) analyzed links between synchronization and network structure in more detail. He found that an early onset of synchronization and a rapid transition into the fully synchronized state are conflicting demands of the network topology. Local clustering supports the first, whereas global organization facilitates the second. Contrasting their simulations, we did not always reach the maximum synchronized state, mainly due to the reasonably large variation in the NMM parameters. Moreover, our structural network was generated as a Watts and Strogatz model, i.e., built on a ring. Nishikawa and others (2003) established that small-world and scale-free networks will have reduced ability to synchronize as the heterogeneity of their connectivity distribution increases, even though the average network distance between the oscillators became smaller. This agrees with our results that after an increase of the time delay between the nodes synchronization occurred with a stronger coupling strength. Motter and colleagues (2005) showed that directed networks with weighted coupling even synchronize more easily.

Varying the structural network topology by rewiring connections randomly with a probability p and varying α resulted in maximum levels of synchronization that were less for the not fully connected network than for a fully connected network. Transition to a synchronized state happened at a critical value of α and the rewiring probability p had a small effect on synchronization, such that small-world-like networks synchronize a bit 'easier' than ordered networks with the same number of edges. Sotero and others (2007) reproduced realistic EEG rhythms with an extended lumped NMM, using an anatomical connectivity matrix with small-world characteristics. They also found an interaction between the network structure and the ability to synchronize. Increasing the delay between the different NMMs only resulted in an increase of the value for α for which the transition occurred.

Finally we compared the underlying structural network topology with the functional connectivity. The results clearly depended on the definition of adjacency given a certain functional connectivity matrix. When fixing the resulting functional network's average degree, the most obvious finding was that for an intermediate range of α the functional path length λ increased as a function of p of the structural network, where γ decreased (see Fig. 6a and b). The path lengths of the functional network were much longer than their surrogate controls, i.e., corresponding to a more structured network, when the underlying structural network became more random. Here, one can conclude that a given structural network configuration does not necessarily lead to a similar functional network configuration. By

contrast, when using a quite conservative criterion to discard all non-significant connections the topological characteristics of structural and functional networks appeared to match better than in the fixed-degree case. Importantly though, using this conservative approach the average degree of the two networks did not necessarily agree. The average degree influences the mean clustering coefficient and the characteristic path length; hence, differences between networks may not necessarily imply a difference in topology, thereby rendering comparison of the structural and functional topologies inherently troublesome.

In general, the relationship between the structural and functional levels may not be fixed, but can depend on network parameters such as the strength of coupling between nodes. Honey and colleagues (2007) suggested that at a slow time scale (minutes of data) the strength of functional coupling between regions is a good indicator for the underlying structural links, whereas on shorter time scales spontaneous functional dynamical changes occurred. This latter result might explain why a random structural network could still produce a structured functional network (large path length) in our study, where we used relatively short epochs of 8.19 s. Recently, Rubinov and colleagues (2009) showed in a model study that coupled chaotic dynamics generate ordered and modular functional patterns, even on a random underlying structural connectivity. They observed that random structural connectivity is reshaped by ordered functional connectivity towards modular topology via rewiring random connections towards nodes with higher synchronization.

A drawback of many studies using 'realistic' models like the current one is the inclusion of a fairly large number of parameters, of which only a limited set can be investigated to keep the study accessible. The number of nodes in the network is one of them, which we chose to be reasonably small.[6] As we looked for a non-trivial structural–functional relationship, we chose to vary parameters that appeared most obvious in this respect, e.g., the coupling strength between NMMs, the number of edges in the structural network and its topology (degree of randomness).

Conclusion

Structural network properties like the coupling strength and network topology can influence functional connectivity patterns. The relation between the two levels is non-trivial as it depends on interplay between the structural topology and coupling strength. This result might have profound impact on the interpretation of studies on functional connectivity that utilize techniques such as EEG, MEG, or fMRI. Drawing clear-cut conclusions from studies that tempt to characterize the neural network solely on the basis of functional measures appears more challenging than before. What causes changes in functional connectivity as found in various pathological conditions like Alzheimer's disease, epilepsy, or brain tumors? Our findings reveal that a loss of synchronization, or a change in functional connectivity patterns, does not necessarily implicate changes at a structural level.

Acknowledgments

We thank Els van Deventer for the literature research. S.C.P. is financially supported by the Dutch Epilepsy fund (NEF grant 05-12). A.D. thanks the Netherlands Organisation for Scientific Research for financial support (NWO grant 452-04-344).

[6] We note again that our results appeared not to depend critically on network size, since we repeated one simulation with $n = 128$ and obtained very similar results; see Supplementary Figs. 2 and 3.

Appendix A. Supplementary data

Supplementary data associated with this article can be found, in the online version, at doi:10.1016/j.neuroimage.2009.10.049.

References

Aertsen, A.M.H.J., Gerstein, G.L., Habib, M.K., Palm, G., 1989. Dynamics of neuronal firing correlation—modulation of effective connectivity. J. Neurophysiol. 61, 900–917.
Ansari-Asl, K., Senhadji, L., Bellanger, J.J., Wendling, F., 2006. Quantitative evaluation of linear and nonlinear methods characterizing interdependencies between brain signals. Phys. Rev. E 031916, 74.
Babiloni, C., Ferri, R., Moretti, D.V., Strambi, A., Binetti, G., Dal Forno, G., Ferreri, F., Lanuzza, B., Bonato, C., Nobili, F., Rodriguez, G., Salinari, S., Passero, S., Rocchi, R., Stam, C.J., Rossini, P.M., 2004. Abnormal fronto-parietal coupling of brain rhythms in mild Alzheimer's disease: a multicentric EEG study. Eur. J. Neurosci. 19, 2583–2590.
Barabasi, A.L., Albert, R., 1999. Emergence of scaling in random networks. Science 286, 509–512.
Bartolomei, F., Bosma, I., Klein, M., Baayen, J.C., Reijneveld, J.C., Postma, T.J., Heimans, J.J., van Dijk, B.W., de Munck, J.C., de Jongh, A., Cover, K.S., Stam, C.J., 2006. Disturbed functional connectivity in brain tumour patients: evaluation by graph analysis of synchronization matrices. Clin. Neurophysiol. 117, 2039–2049.
Boccaletti, S., Latora, V., Moreno, Y., Chavez, M., Hwang, D.U., 2006. Complex networks: structure and dynamics. Physics Reports 424, 175–308.
Brede, M., 2008. Locals vs. global synchronization in networks of non-identical Kuramoto oscillators. European Physical Journal B 62, 87–94.
Chen, M., Shang, Y., Zou, Y., Kurths, J., 2008. Synchronization in the Kuramoto model: a dynamical gradient network approach. Phys. Rev. E. 027101, 77.
Damoiseaux, J.S., Rombouts, S.A.R.B., Barkhof, F., Scheltens, P., Stam, C.J., Smith, S.M., Beckmann, C.F., 2006. Consistent resting-state networks across healthy subjects. Proc. Natl. Acad. Sci. U.S.A. 103, 13848–13853.
David, O., Friston, K.J., 2003. A neural mass model for MEG/EEG: coupling and neuronal dynamics. Neuroimage 20, 1743–1755.
David, O., Cosmelli, D., Hasboun, D., Garnero, L., 2003. A multitrial analysis for revealing significant corticocortical networks in magnetoencephalography and electroencephalography. Neuroimage 20, 186–201.
David, O., Harrison, L., Friston, K.J., 2005. Modelling event-related responses in the brain. Neuroimage 25, 756–770.
Deco, G., Jirsa, V.K., Robinson, P.A., Breakspear, M., Friston, K., 2008. The dynamic brain: from spiking neurons to neural masses and cortical fields. PLoS Comput. Biol. 4, e1000092.
Eguiluz, V.M., Chialvo, D.R., Cecchi, G.A., Baliki, M., Apkarian, A.V., 2005. Scale-free brain functional networks. Phys. Rev. Lett. 018102, 94.
Freeman, W.J., 1978. Models of the dynamics of neural populations. Electroencephalograph. Clin. Neurophysiol. Suppl. 9–18.
Friston, K.J., 2001. Brain function, nonlinear coupling, and neuronal transients. Neuroscientist 7, 406–418.
Golomb, D., Hansel, D., 2000. The number of synaptic inputs and the synchrony of large, sparse neuronal networks. Neural Comput. 12, 1095–1139.
He, Y., Chen, Z.J., Evans, A.C., 2007. Small-world anatomical networks in the human brain revealed by cortical thickness from MRI. Cereb. Cortex 17, 2407–2419.
Hilgetag, C.C., Burns, G.A.P.C., O'Neill, M.A., Scannell, J.W., Young, M.P., 2000. Anatomical connectivity defines the organization of clusters of cortical areas in the macaque monkey and the cat. Philos. Trans. R. Soc. Lond B Biol. Sci. 355, 91–110.
Honey, C.J., Sporns, O., 2008. Dynamical consequences of lesions in cortical networks. Hum. Brain Mapp. 29, 802–809.
Honey, C.J., Kotter, R., Breakspear, M., Sporns, O., 2007. Network structure of cerebral cortex shapes functional connectivity on multiple time scales. Proc. Natl. Acad. Sci. U.S.A. 104, 10240–10245.
Honey, C.J., Sporns, O., Cammoun, L., Gigandet, X., Thiran, J.P., Meuli, R., Hagmann, P., 2009. Predicting human resting-state functional connectivity from structural connectivity. Proc. Natl. Acad. Sci. U.S.A. 106, 2035–2040.
Izhikevich, E.M., Edelman, G.M., 2008. Large-scale model of mammalian thalamocortical systems. Proc. Natl. Acad. Sci. U.S.A. 105, 3593–3598.
Jansen, B.H., Rit, V.G., 1995. Electroencephalogram and visual evoked potential generation in a mathematical model of coupled cortical columns. Biol. Cybern. 73, 357–366.
Kuramoto, Y., 1975. Self-entrainment of a population of coupled non-linear oscillators. In: Arakai, H. (Ed.), International Symposium on Mathematical Problems in Theoretical Physics, Lecture Notes in Physics, pp. 420–422. Springer-Verlag, Kyoto/Japan.
Le Van Quyen, M., 2003. Disentangling the dynamic core: a research program for a neurodynamics at the large-scale. Biological Research 36, 67–88.
Le Van Quyen, M., Foucher, J., Lachaux, J., Rodriguez, E., Lutz, A., Martinerie, J., Varela, F.J., 2001. Comparison of Hilbert transform and wavelet methods for the analysis of neuronal synchrony. J. Neurosci. Methods 111, 83–98.
Lee, L., Harrison, L.M., Mechelli, A., 2003. A report of the functional connectivity workshop, Düsseldorf 2002. Neuroimage 19, 457–465.
Lopes da Silva, F.H., 1991. Neural mechanisms underlying brain waves: from neural membranes to networks. Electroencephalogr. Clin. Neurophysiol 79, 81–93.
Lopes da Silva, F.H., Hoeks, A., Smits, H., Zetterberg, L.H., 1974. Model of brain rhythmic activity. The alpha-rhythm of the thalamus. Kybernetik. 15, 27–37.

Lopes da Silva, F.H., van Rotterdam, A., Barts, P., van Heusden, E., Burr, W., 1976. Models of neuronal populations: the basic mechanisms of rhythmicity. Prog. Brain Res. 45, 281–308.
Lopes da Silva, F.H., Pijn, J.P., Velis, D., Nijssen, P.C., 1997. Alpha rhythms: noise, dynamics and models. Int. J. Psychophysiol. 26, 237–249.
Mardia, K.V., 1972. Statistics of directional data. Academic Press, London.
Maslov, S., Sneppen, K., 2002. Specificity and stability in topology of protein networks. Science 296, 910–913.
Micheloyannis, S., Pachou, E., Stam, C.J., Breakspear, M., Bitsios, P., Vourkas, M., Erimaki, S., Zervakis, M., 2006. Small-world networks and disturbed functional connectivity in schizophrenia. Schizophr. Res. 87, 60–66.
Mormann, F., Lehnertz, K., David, P., Elger, C.E., 2000. Mean phase coherence as a measure for phase synchronization and its application to the EEG of epilepsy patients. Physica D-Nonlinear Phenomena 144, 358–369.
Motter, A.E., Zhou, C.S., Kurths, J., 2005. Enhancing complex-network synchronization. Europhysics Letters 69, 334–340.
Newman, M.E.J., 2003. The structure and function of complex networks. Siam Rev 45, 167–256.
Nishikawa, T., Motter, A.E., Lai, Y.C., Hoppensteadt, F.C., 2003. Heterogeneity in oscillator networks: are smaller worlds easier to synchronize? Phys. Rev. Lett. 014101, 91.
Ponten, S.C., Bartolomei, F., Stam, C.J., 2007. Small-world networks and epilepsy: graph theoretical analysis of intracerebrally recorded mesial temporal lobe seizures. Clin. Neurophysiol. 118, 918–927.
Posthuma, D., de Geus, E.J.C., Mulder, E.J.C.M., Smit, D.J.A., Boomsma, D.I., Stam, C.J., 2005. Genetic components of functional connectivity in the brain: the heritability of synchronization likelihood. Hum. Brain Mapp. 26, 191–198.
Reijneveld, J.C., Ponten, S.C., Berendse, H.W., Stam, C.J., 2007. The application of graph theoretical analysis to complex networks in the brain. Clin. Neurophysiol 118, 2317–2331.
Robinson, P.A., Rennie, C.J., Rowe, D.L., O'Connor, S.C., Gordon, E., 2005. Multiscale brain modelling. Philos. Trans. R. Soc. Lond B Biol. Sci. 360, 1043–1050.
Rosenblum, M.G., Pikovsky, A.S., Kurths, J., 1996. Phase synchronization of chaotic oscillators. Phys. Rev. Lett. 76, 1804–1807.
Rubinov, M., Sporns, O., van Leeuwen, C., Breakspear, M., 2009. Symbiotic relationship between brain structure and dynamics. BMC Neuroscience 10, 55. doi:10.1186/1471-2202-10-55.
Schnitzler, A., Gross, J., 2005. Normal and pathological oscillatory communication in the brain. Nat. Rev. Neurosci. 6, 285–296.
Schuuring, D., 1988. Modelleren en simuleren van epileptische aktiviteit, Master thesis communicatietechniek, Informatie en Systeemtheorie, technische Universiteit Twente [dissertation].
Smit, D.J.A., Stam, C.J., Posthuma, D., Boomsma, D.I., Geus de, E.J.C., 2007. Heritability of "small-world" networks in the brain: a graph theoretical analysis of resting-state EEG functional connectivity. Hum. Brain Mapp. 29, 1368–1378.
Sotero, R.C., Trujillo-Barreto, N.J., Iturria-Medina, Y., Carbonell, F., Jimenez, J.C., 2007. Realistically coupled neural mass models can generate EEG rhythms. Neural Comput 19, 478–512.
Sporns, O., Zwi, J.D., 2004. The small world of the cerebral cortex. Neuroinformatics 2, 145–162.
Sporns, O., Tononi, G., Edelman, G.M., 2000. Connectivity and complexity: the relationship between neuroanatomy and brain dynamics. Neural Netw. 13, 909–922.
Stam, C.J., Pijn, J.P., Suffczynski, P., Lopes da Silva, F.H., 1999a. Dynamics of the human alpha rhythm: evidence for non-linearity? Clin. Neurophysiol. 110, 1801–1813.
Stam, C.J., Vliegen, J.H., Nicolai, J., 1999b. Investigation of the dynamics underlying periodic complexes in the EEG. Biol. Cybern. 80, 57–69.
Stam, C.J., Breakspear, M., van Cappellen, A.M., van Dijk, B.W., 2003. Nonlinear synchronization in EEG and whole-head MEG recordings of healthy subjects. Hum. Brain Mapp. 19, 63–78.
Stam, C.J., Montez, T., Jones, B.F., Rombouts, S.A., van der, Made, Y., Pijnenburg, Y.A., Scheltens, P., 2005. Disturbed fluctuations of resting state EEG synchronization in Alzheimer's disease. Clin. Neurophysiol. 116, 708–715.
Stam, C.J., Jones, B.F., Nolte, G., Breakspear, M., Scheltens, P., 2007a. Small-world networks and functional connectivity in Alzheimer's disease. Cereb. Cortex 17, 92–99.
Stam, C.J., Nolte, G., Daffertshofer, A., 2007b. Phase lag index: assessment of functional connectivity from multi channel EEG and MEG with diminished bias from common sources. Hum. Brain Mapp. 28, 1178–1193.
Stam, C.J., de Haan, W., Daffertshofer, A., Jones, B.F., Manshanden, I., van Cappellen, A.M., Montez, T., Verbunt, J.P., de Munck, J.C., van Dijk, B.W., Berendse, H.W., Scheltens, P., 2008. Graph theoretical analysis of magnetoencephalographic functional connectivity in Alzheimer's disease. Brain 132, 213–224.
Stephan, K.E., Hilgetag, C.C., Burns, G.A., O'Neill, M.A., Young, M.P., Kötter, R., 2000. Computational analysis of functional connectivity between areas of primate cerebral cortex. Philos. Trans. R. Soc. Lond B Biol. Sci. 355, 111–126.
Stephan, K.E., Riera, J.J., Deco, G., Horwitz, B., 2008. The Brain Connectivity Workshops: moving the frontiers of computational systems neuroscience. Neuroimage 42, 1–9.
Uhlhaas, P.J., Singer, W., 2006. Neural synchrony in brain disorders: relevance for cognitive dysfunctions and pathophysiology. Neuron 52, 155–168.
Ursino, M., Zavaglia, M., Astolfi, L., Babiloni, F., 2007. Use of a neural mass model for the analysis of effective connectivity among cortical regions based on high resolution EEG recordings. Biol. Cybern. 96, 351–365.
Valdes, P.A., Jimenez, J.C., Riera, J., Biscay, R., Ozaki, T., 1999. Nonlinear EEG analysis based on a neural mass model. Biol. Cybern. 81, 415–424.
van Wijk, B.C.M., Stam, C.J., Beek, P.J., Daffertshofer, A., in preparation. How to compare graph-measures between networks of different size and density?
van Rotterdam, A., Lopes da Silva, F.H., van den, E.J., Viergever, M.A., Hermans, A.J., 1982. A model of the spatial-temporal characteristics of the alpha rhythm. Bull. Math. Biol. 44, 283–305.
van Vreeswijk, C., 2000. Analysis of the asynchronous state in networks of strongly coupled oscillators. Physical Review Letters 84, 5110–5113.
Varela, F., Lachaux, J.P., Rodriguez, E., Martinerie, J., 2001. The brainweb: phase synchronization and large-scale integration. Nat. Rev. Neurosci. 2, 229–239.
Wang, X.F., Chen, G., 2003. Complex networks: small-world, scale-free and beyond. IEEE Circuits and systems magazine 6–20.
Watts, D.J., Strogatz, S.H., 1998. Collective dynamics of 'small-world' networks. Nature 393, 440–442.
Wendling, F., Bartolomei, F., Bellanger, J.J., Chauvel, P., 2001. Interpretation of interdependencies in epileptic signals using a macroscopic physiological model of the EEG. Clin. Neurophysiol. 112, 1201–1218.
Wendling, F., Hernandez, A., Bellanger, J.J., Chauvel, P., Bartolomei, F., 2005. Interictal to ictal transition in human temporal lobe epilepsy: insights from a computational model of intracerebral EEG. J Clin. Neurophysiol. 22, 343–356.
Wilson, H.R., Cowan, J.D., 1972. Excitatory and inhibitory interactions in localized populations of model neurons. Biophys. J. 12, 1–24.
Yu, S., Huang, D., Singer, W., Nikolic, D., 2008. A small world of neuronal synchrony. Cereb. Cortex 18, 2891–2901.
Zetterberg, L.H., Kristiansson, L., Mossberg, K., 1978. Performance of a model for a local neuron population. Biol. Cybern. 31, 15–26.
Zhou, C., Zemanova, L., Zamora, G., Hilgetag, C.C., Kurths, J., 2006. Hierarchical organization unveiled by functional connectivity in complex brain networks. Phys. Rev. Lett. 238103, 97.
Zhou, C.S., Zemanova, L., Zamora-Lopez, G., Hilgetag, C.C., Kurths, J., 2007. Structure–function relationship in complex brain networks expressed by hierarchical synchronization. New Journal of Physics 9, 1–21.